Thin-Walled Structures 48 (2010) 935–945

Contents lists available at ScienceDirect

Thin-Walled Structures

journal homepage: www.elsevier.com/locate/tws

Challenges in the computation of lower-bound buckling loads for tanks under wind pressures

Eduardo M. Sosa [a], Luis A. Godoy [b,*]

[a] Department of Civil and Environmental Engineering, West Virginia University, P.O. Box 6103, Morgantown, WV, USA
[b] CONICET and Structures Department, FCEFyN, Universidad Nacional de Córdoba, Casilla de Correo 916, Córdoba 5000, Argentina

ARTICLE INFO

Article history:
Received 26 April 2010
Received in revised form
30 June 2010
Accepted 30 June 2010
Available online 23 July 2010

Keywords:
Buckling
Non-linear analysis
Reduced energy method
Tanks
Wind pressure

ABSTRACT

This paper reports on the implementation of a lower-bound approach for the buckling of imperfection-sensitive shells using general purpose finite element codes. The stability of cylindrical steel tanks under wind pressure is evaluated for two tank configurations: conical roof tanks and open top tanks. For both tank configurations, several geometric relations are considered in order to find the variation of the knock-down factor as the geometry changes. The reduced energy method is implemented to compute a lower-bound for critical wind pressures and the results are compared with the static non-linear analysis carried out on the same models. An alternative way to implement the reduced energy method is presented to improve the results obtained with the proposed methodology.

1. Introduction

Large thin-walled tanks are employed by various industries to mainly store oil, water and petrochemical products. During weather events involving high wind speeds such as in hurricanes, the occurrence of moderate damage to total failure is mainly associated with buckling of cylindrical shell of the tank [1,2]. It is well known that the buckling behavior of shells is sensitive to initial imperfections, which produces a drop in the critical load. This drop may be moderate, as in laterally loaded cylinders and cylindrical panels, or severe, as in axially loaded cylinders and pressurized spherical shells [3,4].

Some of the studies on the effect of wind pressures on cylindrical shells include analysis mainly carried out on silos using classical analytical formulations as in [4–6] or in short open top tanks analyzed by finite element models. For example, Godoy and Flores [7,8] studied imperfection-sensitivity to elastic buckling of wind loaded open cylindrical tanks; Portela and Godoy [9] used both bifurcation analysis and geometrical non-linear analysis for buckling of tanks with conic roof under wind load.

Typically, imperfection-sensitivity on shells is analyzed by geometrical non-linear analysis, but this methodology is computationally expensive and not always available. However, there are alternative ways to account for imperfection-sensitivity, and one of the most interesting approaches oriented to shell design has been the lower bound theory based on a reduced-energy model of the shell developed by Croll and co-workers [10–14]. In the reduced-energy approach it is important to identify the energy components of the shell in the classical eigenmodes, including membrane and bending components as well as load potentials. Depending on the shell and load system, some of the contributions to the second variation of the total potential energy are positive and others are negative, which means that they are stabilizing or de-stabilizing components. The main hypothesis is that stabilizing (positive) components may be lost in the shell due the presence of imperfections. Thus, the reduced energy approach uses a simplified energy version in which some stabilizing components are eliminated from the initial post-critical condition. This lower-bound theory has been validated extensively for many shell forms [10–14]. Sosa et al. [15] investigated the implementation of a lower-bound approach for the buckling of imperfection-sensitive shells using general purpose finite element codes for cylindrical shells with different geometric configurations under uniform pressure. The lower-bound approach can be expressed in terms of reduced stiffness, as well. Jaca et al. [16] reported on a reduced stiffness approach for the buckling of open cylindrical tanks subjected to wind loads to compute the lower-bound buckling loads.

This work aims to show the results of the implementation of the reduced-energy approach in conjunction with a general purpose finite element program to compute the lower-bound buckling loads for tanks with different geometric configurations and subjected to non-uniform (wind) pressures.

* Corresponding author.
E-mail addresses: lgodoy@com.uncor.edu, luis.godoy@upr.edu (L.A. Godoy).

0263-8231/$ - see front matter © 2010 Elsevier Ltd. All rights reserved.
doi:10.1016/j.tws.2010.06.004

2. Conical roof tanks under wind pressure

Initially, six conical roof tanks models are considered for computing the lower-bound buckling loads. These models are identified as MC1, MC2, MC3, MC4, MC5 and MC6. The cylindrical part of the models has variable height, ranging from $H/D=0.24$ to 0.95, with tapered thickness calculated according the 1-foot method specified in the API-650 [17]. The material is steel, with elastic modulus $E=206$ GPa and Poisson ratio $v=0.3$.

All the models have a conical fixed roof supported by 32 rafters with a roof slope of 3/16. The cylinder is assumed to be fixed at the base and it is assumed that each model is isolated, so that the pressures applied on the shell and on the roof are not perturbed by other surrounding tanks. Tables 1 and 2 summarize all the information regarding the dimensions adopted for the models. Fig. 1 shows the geometry of all the models considered in this section.

Table 1
Dimensions adopted for the cylindrical part of the model.

	MC1	MC2	MC3	MC4	MC5	MC6
H (m)	7.32	12.19	17.07	19.20	24.08	28.96
D (m)	30.48	30.48	30.48	30.48	30.48	30.48
H/D	0.24	0.40	0.56	0.63	0.79	0.95

Table 2
Thicknesses adopted for each model.

Course	MC1	MC2	MC3	MC4	MC5	MC6
	t_{design} (m)	t_{design} (m)	t_{design} (m)	t_{design} (m)	t_{design} (m)	t_{design} (m)
1	0.0095	0.0127	0.0175	0.0206	0.0254	0.0286
2	0.0079	0.0111	0.0159	0.0175	0.0222	0.0254
3	0.0079	0.0079	0.0127	0.0159	0.0206	0.0254
4		0.0079	0.0111	0.0127	0.0175	0.0222
5		0.0079	0.0095	0.0111	0.0159	0.0206
6			0.0079	0.0079	0.0127	0.0191
7			0.0079	0.0079	0.0111	0.0159
8				0.0079	0.0079	0.0127
9					0.0079	0.0111
10					0.0079	0.0079
11						0.0079
12						0.0079

The space variation of pressures in the cylindrical part of the tank is assumed to be constant in elevation and variable around the circumference, as in other research works in the field [5,9]. For the pressures acting on the roof, this section considers the wind-tunnel pressures obtained by Mac Donald et al. [18], which are similar to those reported by Portela and Godoy [9]. The maximum pressure in the reference case is taken as 1 KPa acting on the windward meridian on the cylindrical part of the shell. For the stability analysis, the values of the pressures acting on the complete shell are scaled using the load parameter λ. The circumferential pressure distribution is assumed in the form:

$$p = \lambda \sum_{i=0}^{6} c_i \cos(i\theta) \tag{1}$$

where the Fourier coefficients are: $c_0=0.387$, $c_1=-0.338$, $c_2=-0.533$, $c_3=-0.471$, $c_4=-0.166$, $c_5=0.066$ and $c_6=0.055$. Fig. 2(a) shows the pressure distribution used in the conical roof and Fig. 2(b) shows the wind pressure distribution assumed around the circumference.

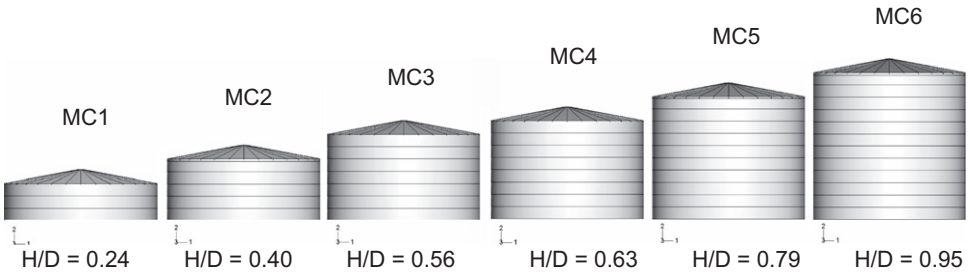

Fig.1. Relative proportions of the models with conical roof.

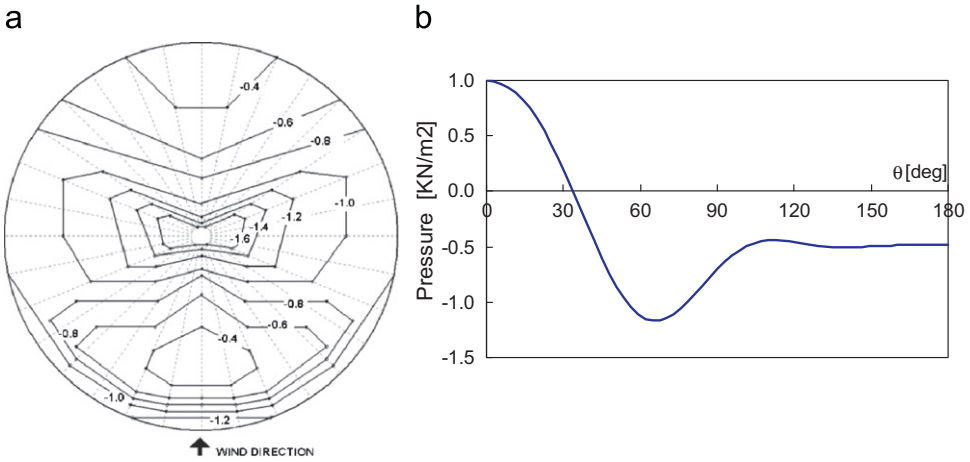

Fig. 2. (a) Pressure distribution used in the conical roof. (b) Wind pressure distribution assumed around the circumference.

2.1. Computational model for classical buckling analysis

All the tanks investigated were modeled by using Abaqus [19]. Meshes were generated by using the triangular element STRI3 [20] with adequate density to obtain convergence. The computations are divided in three stages: first, the critical load is calculated by solving the classical buckling eigenproblem; second, the methodology of reduced energy is implemented; and third, non-linear analyses with geometric imperfections are carried out to compare the results with those obtained in the second step.

Results obtained from the classical eigenvalue problem show that the eigenvalues for the first and second modes are practically the same for all the models studied. The shortest model (MC1) seems to be more rigid and the classical critical loads in the other models (MC2–MC6) tend to a constant value as the relation H/D increases. Table 3 summarizes the eigenvalues for the modes 1 and 2.

In order to relate the critical pressures indicated in Table 3 to wind speed, it is possible to use ASCE-7-02[21] to calculate the wind speed associated to the critical pressures:

$$p_{cr} = 0.613 K_z K_{zt} K_d I V^2 \tag{2}$$

where p_{cr} is the critical pressure of the wind in (N/m^2), V is the basic wind speed (m/s), K_z is the exposition factor, K_{zt} is the topographic factor, K_d is the directionality factor and I is the importance factor. It is assumed that the tanks are placed in flat terrain, so $K_{zt}=1$. Category II structure gives the importance factor $I=1$, the directionality factor $K_d=1$ and $K_z=0.94$; then Eq. (2) becomes

$$p_{cr} = 0.576 V^2 \tag{3}$$

Wind speeds shown in Table 3 were calculated using Eq. (3).

Table 3
Critical pressures for wind loaded tanks.

Model		Critical pressure (kN/m^2)		Critical wind gust speed (Km/h)
		Mode 1	Mode 2	
MC1	$H/D=0.24$	3.854	3.881	294
MC2	$H/D=0.40$	2.480	2.481	236
MC3	$H/D=0.56$	2.916	2.926	256
MC4	$H/D=0.63$	2.537	2.547	239
MC5	$H/D=0.79$	2.558	2.568	240
MC6	$H/D=0.95$	2.478	2.485	236

2.2. Computational model for reduced energy analysis

In this step, the lower-bound wind pressure is calculated using the first mode of the eigenvalue analysis as an imposed displacement pattern. Every part of the shell that forms the whole cylinder (all courses) undergoes simultaneous reductions in the membrane stiffness while the scaled mode is imposed as a prescribed initial displacement. In that configuration, the energy used by the structure to reach that deflected configuration is calculated [15]. With the calculated energy for each reduction factor α eroding the membrane stiffness and having calculated the energy without reduction in its stiffness for the same load conditions, we are able to determine the loss in the buckling capacity to support additional load. The knock-down factor η is defined as the ratio between the energy computed for different levels of reduction in the membrane stiffness and the energy computed with all the membrane stiffness, say $\eta = U_b/(U_m+U_b)$.

The computation of energies shows that the knock-down factor η tends to a constant value as the reduction factor α increases. The results of these computations are illustrated in Fig. 3. From these plots, it seems that the knock-down factor has a small dependence on the H/D relations. All the models show a similar trend and the maximum difference in η between the shortest and the tallest model is only 4%.

2.3. Lower bound via non-linear analysis

To compare the lower bound results with those obtained in the previous classical analysis, non-linear imperfection-sensitivity analyses are carried out. All the models are analyzed including small amplitude imperfections following the shape of the first eigenmode. The amplitudes of the imperfections vary from 0.10 t_{min} to 1.0 t_{min}, where t_{min} is the smallest shell thickness of each cylinder. For each imperfection level, non-linear equilibrium paths are computed using the Riks technique, so that the structure may display its post-critical behavior. For small amplitude imperfections, the non-linear post-critical path is unstable. This means that the shell can withstand a maximum load for a relatively small displacement. Beyond that maximum, the shell cannot take additional loads and it has large deflections.

For imperfection amplitudes larger than 1.0 t_{min}, the equilibrium path has very large deflections, becomes stable and constantly raising. This is an indication that the shape of the shell has changed so much that the behavior is quite different from the behavior of the original perfect shell. This level of

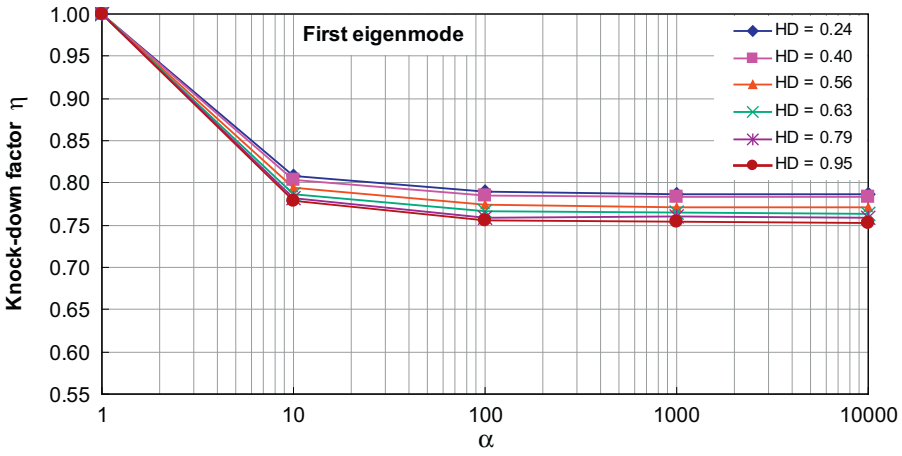

Fig. 3. Knock-down factors calculated using the reduced energy method for the first eigenmode.

imperfection settles on the lower limit of load that the structure is able to support with small deviations from the original form. After that limit, the deflected structure behaves in a different way.

Typical non-linear equilibrium paths for the mentioned levels of imperfections are shown for the models MC2, MC4 and MC6 in Fig. 4. The imperfection-sensitivity curves shown in the right side

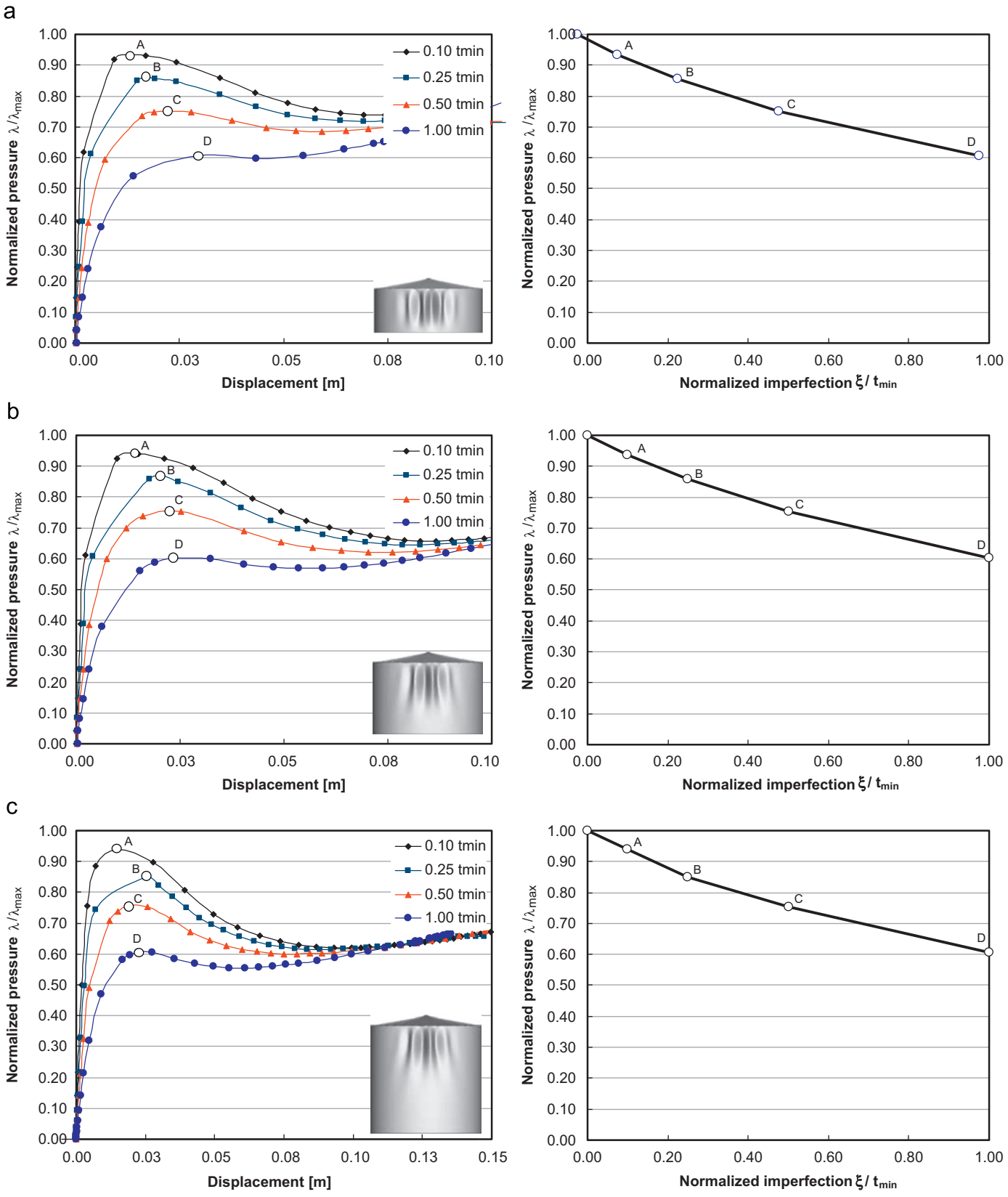

Fig. 4. Non-linear equilibrium paths and imperfection-sensitivity curves obtained using first buckling mode as imperfection shape: (a) MC2 ($H/D=0.40$); (b) MC4 ($H/D=0.63$); and (c) MC6 ($H/D=0.95$).

in Fig. 4 were generated by plotting the normalized critical load λ/λ_{max} for each imperfection level versus the dimensionless imperfection amplitude ξ/t_{min}. Fig. 5 summarizes all those curves for all the models analyzed and they show the lower limit to which the pressure loads tend as the imperfection levels increase. In this way, the knock-down factor $\eta=\lambda/\lambda_{max}$ is directly comparable with the results obtained using the reduced energy method.

From Fig. 5 it is seen that the imperfection-sensitivity is practically the same for all the models. This feature may be justified by the fact that in all the models the buckling mode deflections are concentrated in the upper part of the tanks, which corresponds to the zone of lower shell thickness. This thickness is the minimum required by the design in all models and at least the last three courses at the top of the cylinder have the minimum thickness. Probably, that is why the classic eigenvalues indicated in Table 3 have small variations as the H/D ratio increases.

Notice that the knock-down factor in Fig. 5 does not approach clearly a plateau as obtained in the reduced energy method depicted in Fig. 3. Comparing the results displayed in Figs. 3 and 5, the reduced energy method predicts higher lower limits than those shown by the imperfection-sensitivity analysis. In the reduced energy method, the curves tend to values of η ranging from 0.758 to 0.785, while in the non-linear analysis method, for the maximum imperfection amplitude considered ($\xi/t_{min}=1.00$), the lower limit considering both modes seems to be between 0.6 and 0.7.

Clearly, the values predicted by the proposed reduced energy method for wind pressures cannot be considered a safe lower limit. The main reason for the discrepancy seems to be associated with the different deflection modes obtained in the classical eigenvalue and the non-linear analyses. The first mode obtained in the classical eigenvalue computations (and then used in the reduced energy method) is not quite the same as the mode found in the non-linear analysis with an imperfection as illustrated in Fig. 6.

3. Open tanks under wind pressure

The models analyzed in this section are the same as those considered by Godoy and Flores [7]. There are four cantilever cylinders with different geometric relations studied in order to emphasize the differences in the behavior according to changes in their geometric relations. These models represent tanks clamped at the base and free at the upper edge without any reinforcing ring and with constant thickness. The material is steel, with elastic modulus $E=206$ GPa and Poisson ratio $\nu=0.3$. The main geometric properties for the models are summarized in Table 4

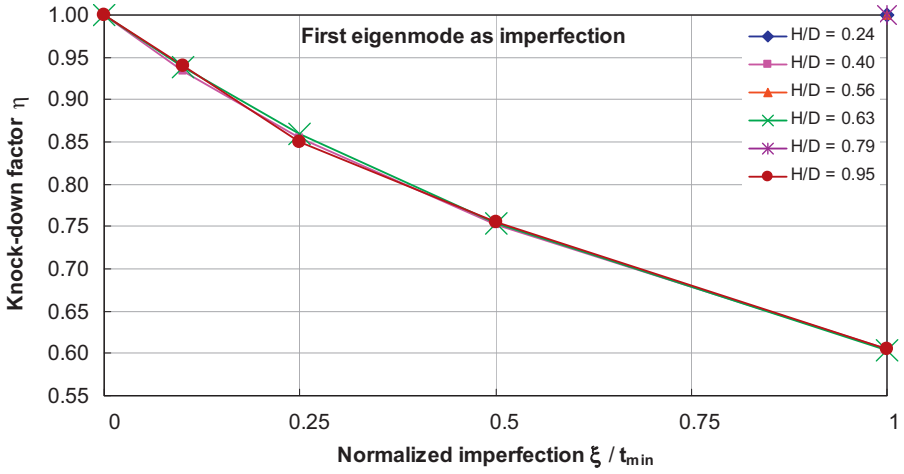

Fig. 5. Knock-down factor calculated with non-linear imperfection-sensitivity analysis using the first eigenmode as imperfection shape.

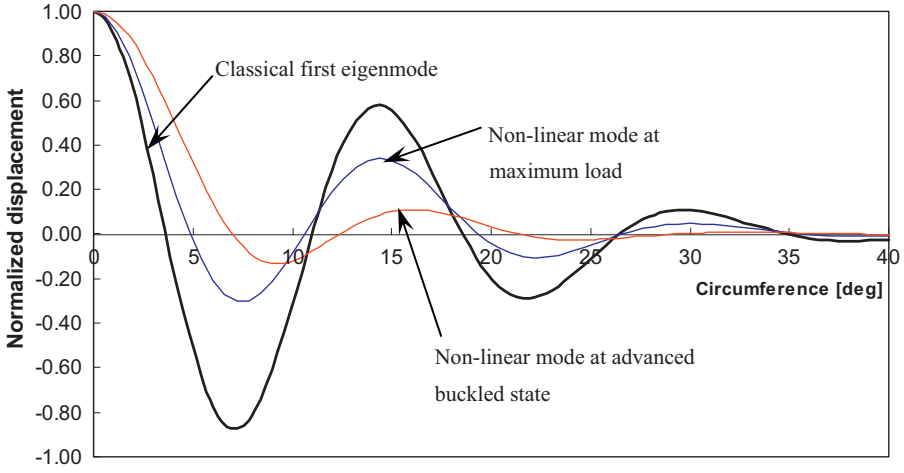

Fig. 6. Comparison of buckling modes.

where Z is the Batdorf parameter given by

$$Z = \frac{H^2}{Rt}\sqrt{(1-\nu^2)} \tag{4}$$

where H is the height, R the radius, t the thickness and ν the Poisson's coefficient. The Batdorf parameter is a measure of the slenderness of the cylindrical shell and as its value increases, the slenderness of the shell increases. Fig. 7 provides a graphical representation of the geometries. The discretization of the shells is carried out using STRI3 finite elements and the load distribution in the cylindrical shell is the same as that used for the conical roof tanks.

3.1. Computational model for classical buckling analysis

For the set of open tanks described above, classical linear buckling analysis was performed. For the wind pressures given by Eq. (1), the classical critical pressures were calculated and contrasted with the results reported in [7]. To understand the influence of the specific finite element employed, the critical values were also calculated using S8R5 elements. The results obtained with the proposed discretization using STRI3 elements predict values are close to those calculated with S8R5 elements, and they are in good agreement with the previously reported results [7]. Table 5 summarizes the results.

Table 4
Open tanks: geometric properties.

Model	Diameter	Height	Thickness	Non-dimensional parameters		
	D (m)	H (m)	t (m)	H/D	R/t	Z
M1	24.0	4.0	0.006	0.17	2000	212
M2	14.0	3.5	0.004	0.25	1750	417
M3	9.0	4.5	0.003	0.50	1500	1431
M4	5.0	5.0	0.002	1.00	1250	4770

3.2. Lower bound using reduced energy method

As in the conical roof models, the deflections in the buckled mode are concentrated in the windward zone and the suction has almost no effect on the deflected shape. Also, as the slenderness increases, the number of waves decreases and the deflected shape concentrates in the upper zone of the cylinder. Abaqus [19] normalizes the mode using the maximum displacement, so that the maximum normalized displacement is equal to one.

Those normalized first modes were used to calculate the lower bound pressures using the reduced energy method. For convenience, a scaling factor 1/1000 was used for the modes, although using other scaling factors leads to identical results. The knock-down factor $\eta = U_b/(U_m + U_b)$ calculated for each model is illustrated in Fig. 8 where it is seen that the knock-down factor converges to a constant value for α larger than 100 and is practically independent of the model geometry.

3.3. Lower-bound via non-linear analysis

According to the results reported by Godoy and Flores [7], the knock-down factor should lead to different lower bounds as the geometry of the tank changes. However, Fig. 8 shows that all the models tend to approximately the same lower limit. For example, consider just two extreme cases, model M1 ($H/D = 0.17$) and model M4 ($H/D = 1.00$): the reduction factors according to results reported in [7] are approximately $\eta_{M1} = 0.60$ and $\eta_{M4} = 0.95$. Those results have been reproduced with the models used here (see Fig. 9), using element STRI3 and geometrical non-linear analysis. Clearly, the lower bound estimates shown in the previous section are not in

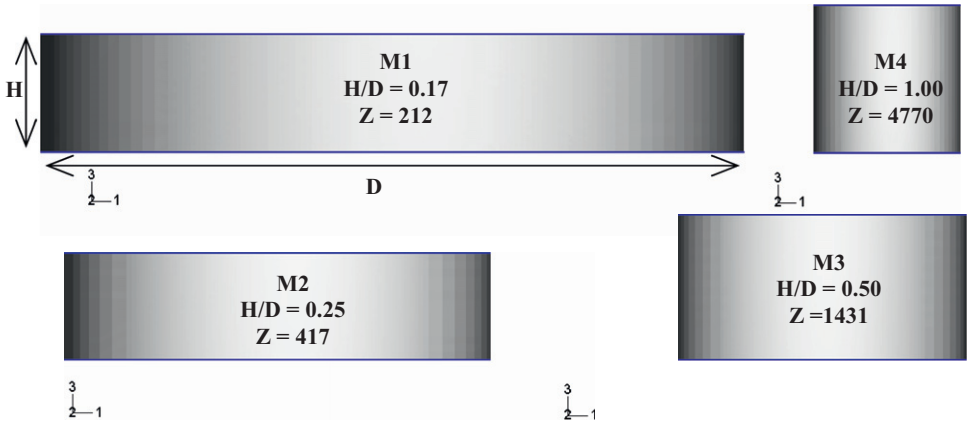

Fig. 7. Relative size of open tank models considered for the analysis.

Table 5
Open tanks: classical critical loads (eigenvalue analysis).

Model	Non-dimensional parameters			λ^c (kN/m2)			Critical wind gust Speed (Km/h)
	H/D	R/t	Z	Ref. [7]	S8R5	STRI3	
M1	0.17	2000	212	2.282	2.201	2.225	225
M2	0.25	1750	417	–	2.107	2.137	220
M3	0.50	1500	1431	–	1.683	1.694	196
M4	1.00	1250	4770	1.558	1.500	1.518	186

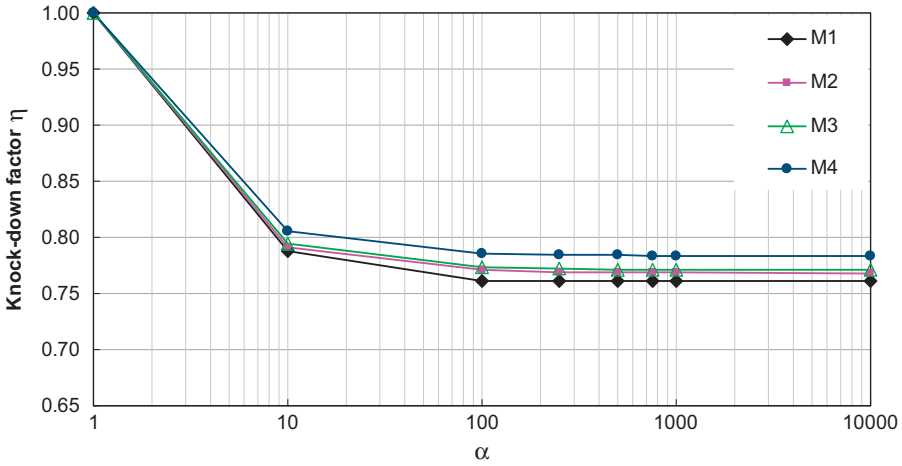

Fig. 8. Lower bound estimate for open tank models.

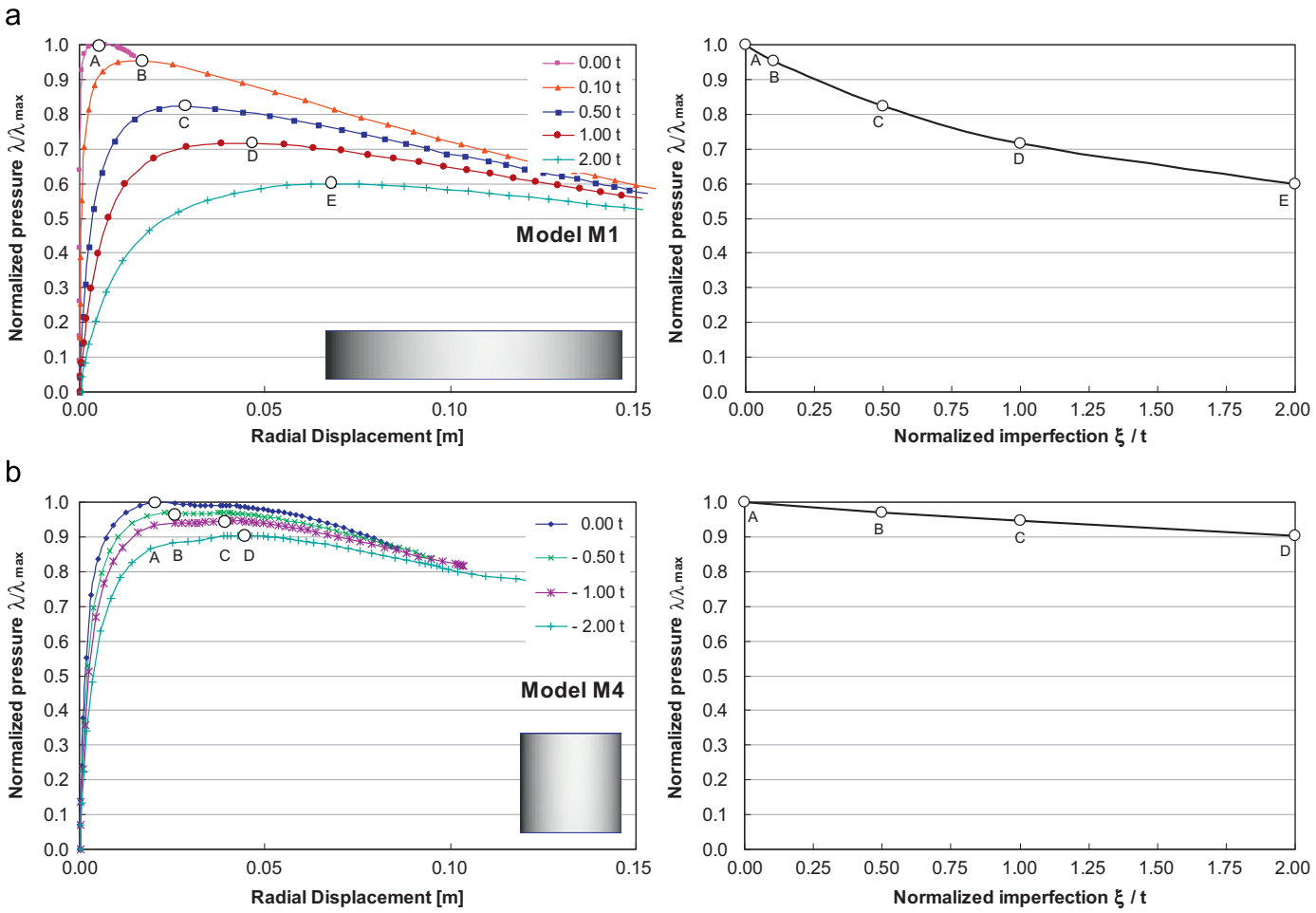

Fig. 9. Results of non-linear imperfection-sensitivity analysis. Imperfection shape: first mode; (a) M1 ($H/D=0.17$) and (b) M4 ($H/D=1.00$).

good agreement with the non-linear results. An alternative for overcoming such differences are proposed in the next section.

4. An alternative for improving the lower bound computations

In sight of the results described in the previous sections, it is apparent that the proposed lower bound approach has not been able to capture the expected behavior displayed in the non-linear analysis. Changes in the mode normalization to compute the energy is proposed here to overcome such differences.

To understand the reasons of the discrepancies in the results, we write the classic eigenvalue problem as

$$\Phi_1^T[K-\lambda_C K_G(N_F)]\Phi_1 = 0 \tag{5}$$

where Φ_1^T is the first eigenmode in the classic eigenvalue analysis, K is the stiffness matrix, K_G is the geometric matrix assembled

with the contributions of the initial stresses N_F in the fundamental state and λ_C is the classical critical load. Matrix K has a membrane (K_m) and a bending (K_b) component, thus

$$\Phi_1^T[(K_m+K_b)-\lambda_C K_G(N_F)]\Phi_1=0 \tag{6}$$

Next, the membrane stiffness is eroded in the reduced eigenproblem, so that the lower bound should be computed as

$$\Phi^{*T}[(K_b)-\lambda^* K_G(N_F)]\Phi^*=0 \tag{7}$$

where Φ^{*T} is the mode in the lower bound state and λ^* is the reduced critical load. Eqs. (6) and (7) can be written in terms of computable energies as

$$\Phi_1^T[(K_m+K_b)]\Phi_1=\lambda_C\Phi_1^T[K_G(N_F)]\Phi_1 \tag{8}$$

$$\Phi^{*T}[(K_b)]\Phi^*=\lambda^*\Phi^{*T}[K_G(N_F)]\Phi^* \tag{9}$$

The left side in Eq. (8) corresponds to the energy computed with the complete contribution of membrane and bending stiffness. The right side of Eq. (8) contains an energy term involving the geometric matrix that is not easily computable because, although the modes are known from the classical eigenproblem, the geometric matrix K_G is not explicitly available in Abaqus. In this case, a different normalization of the eigenvector, similar to what is used in structural dynamics, is to let $\Phi_1^T[K_G(N_F)]\Phi_1=1$. Before the normalization, the scalar

$$\Phi^T[K_G(N_F)]\Phi^*=\psi \tag{10}$$

is used to normalize this term in a way that the energy involving the geometric matrix becomes one. Thus, Eq. (8) takes the following form:

$$\Phi_1^T[(K_m+K_b)]\Phi_1=\lambda_C\psi \tag{11}$$

After normalization, we get a mode $\overline{\Phi}_1=\Phi_1/\sqrt{\psi}$, and

$$\frac{\Phi_1^T}{\sqrt{\psi}}[(K_m+K_b)]\frac{\Phi_1}{\sqrt{\psi}=\lambda_C} \tag{12}$$

From Eq. (12), Abaqus can compute the energy $\Phi_1^T[(K_m+K_b)]\Phi_1$, as well as λ_C; then, the normalization factor ψ is calculated from those values as

$$\psi=\frac{\Phi_1^T[(K_m+K_b)]\Phi_1}{\lambda_C} \tag{13}$$

Repeating the same procedure in Eq. (9), we get:

$$\Phi^{*T}[K_G(N_F)]\Phi^*=\rho \tag{14}$$

Then, the reduced eigenproblem in Eq. (9) becomes

$$\Phi^{*T}[K_b]\Phi^*=\lambda^*\rho \tag{15}$$

or else:

$$\frac{\Phi^{*T}}{\sqrt{\rho}}[K_b]\frac{\Phi^*}{\sqrt{\rho}=\lambda^*} \tag{16}$$

Notice that the normalization factors ρ and ψ are quite different ($\rho\neq\psi$). There are two unknowns in Eq. (15): the reduced eigenvalue λ^*, which is the lower bound, and the mode Φ^* for such reduced eigenvalue. Notice that the main objective of this proposed procedure is to find λ^* as well as Φ^* without using non-linear imperfection analysis.

First, we assume that the reduced eigenmode Φ^* is available from the non-linear analysis. Then, the left side of Eq. (15) can be computed. However, in the other side, even with the assumed Φ^*, ρ is also a function of matrix K_G. This matrix is the same as that used in Eq. (8) because the lower bound must occur along the same fundamental path as the classical critical load, so that the initial stresses in both states must be the same.

The most important unknown is still the reduced eigenvalue λ^* and although the term $\Phi^{*T}[K_b]\Phi^*$ in Eq. (15) can be computed, the absence of λ^* or ρ does not allow to proceed with the computations. An additional condition is needed to overcome that restrictive situation. The key limitation is that Abaqus [19] does not allow the user to compute K_G individually and extract that result separately. Regardless of this limitation, the knock-down factor can be expressed in the form:

$$\eta=\frac{\lambda^*}{\lambda_C}=\frac{\psi}{\rho}\frac{\Phi_1^{*T}[K_b]\Phi_1^*}{\Phi_1^T[(K_m+K_b)]\Phi_1} \tag{17}$$

From this last equation, except for ρ, it is possible to compute all the other terms and the reduction factor would be only a function of a constant multiplied by the inverse of ρ, that is

$$\eta=\frac{\lambda^*}{\lambda_C}=\frac{1}{\rho}C \tag{18}$$

where the constant C is

$$C=\psi\frac{\Phi^{*T}[K_b]\Phi^*}{\Phi_1^T[(K_m+K_b)]\Phi_1} \tag{19}$$

Graphically, Eq. (18) is a hyperbola and contains the values of the normalization factors ψ and ρ. If we rewrite the constant C remembering that

$$\left(\frac{1}{\alpha}K_m+K_b\right)\to K_b \quad \text{as} \quad \alpha\to\infty \tag{20}$$

substituting Eqs. (20) into (19), we get

$$C=\psi\frac{\Phi^{*T}[(1/\alpha)K_m+K_b]\Phi^*}{\Phi_1^T[(K_m+K_b)]\Phi_1} \tag{21}$$

Eq. (21) substituted into Eq. (18) leads to a family of hyperbolas for different values of the reduction factor α, which are illustrated in Figs. 10 and 11 for models M1 and M4, respectively. For our purposes, it is interesting to find the limiting values of ψ and ρ to predict accurate values of η as geometry changes. In the graphs, ψ^C indicates the value for which C is computed with α equal to one, say with no membrane

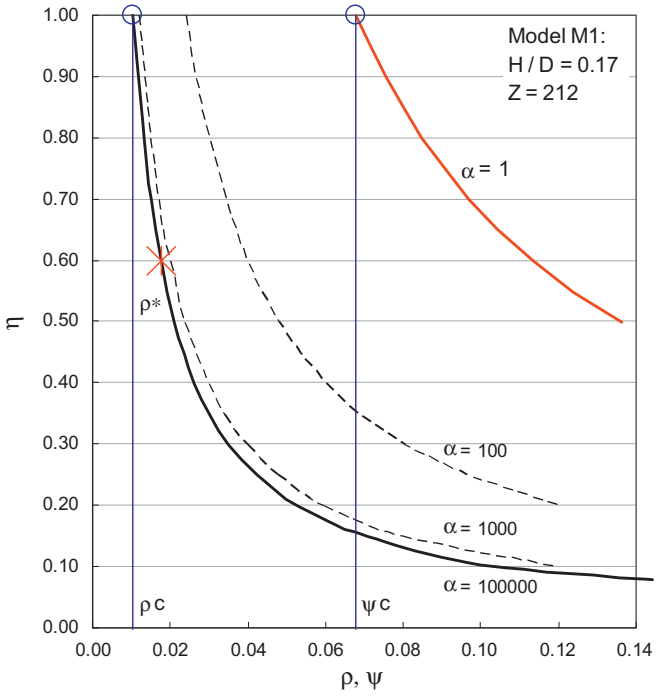

Fig. 10. Variation of η as a function of ψ, ρ and the membrane reduction coefficient α, for model M1.

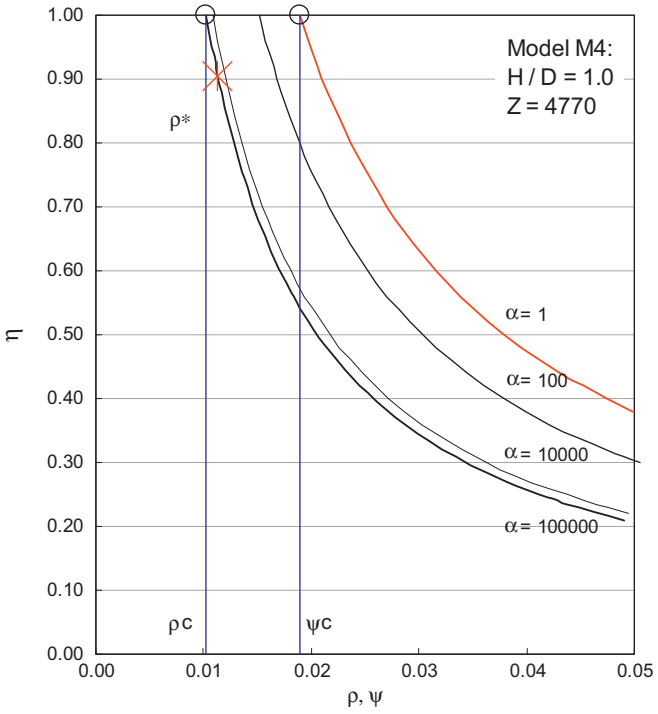

Fig. 11. Variation of η as a function of ψ, ρ and the membrane reduction coefficient α, for model M4.

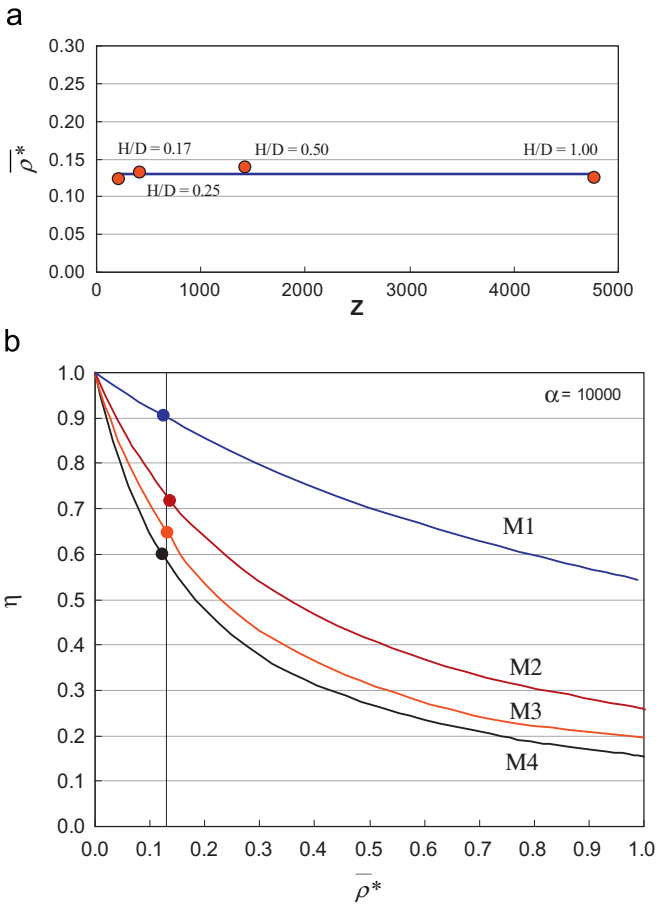

Fig. 12. (a) Variation of $\overline{\rho}*$ as a function of H/D and Z. (b) Variation of η as a function of $\overline{\rho}*$, for all open tank models.

Table 6
Normalized factor for open tank models.

Model	H/D	Z	η	$\overline{\rho}^*$
M1	0.17	212	0.598	0.1228
M2	0.25	417	0.647	0.1324
M3	0.50	1431	0.718	0.1379
M4	1.00	4770	0.904	0.1248

stiffness reduction. Also, ρ^C indicates the value of C for a large reduction in the membrane stiffness, say $\alpha \to \infty$. Then, ρ^* must be between these two values, which is the value that satisfies Eq. (18) for a correct lower bound critical load.

As previously mentioned, an additional condition is needed to find that value in absence of the capability of computing using K_G and mode Φ^*, but this condition is not available from the formulation. However, from Figs. 10 and 11, in the range ψ^C–ρ^C, every value of ρ can be normalized as

$$\overline{\rho} = \frac{\rho - \rho^C}{\psi^C - \rho^C} \tag{22}$$

Particularly, for ρ^* there is a normalized value $\overline{\rho}^*$, given by

$$\overline{\rho}* = \frac{\rho* - \rho^C}{\psi^C - \rho^C} \tag{23}$$

This normalized coefficient indicates how distant is ρ^* from ρ^C according to the model and it is computed for open tank models in order to see if it changes as the geometry and the knock-down factor change.

For open tank models, from Table 6 and Fig. 12(a), it is seen that $\overline{\rho}^*$is about 0.13 and seems to be almost constant for different geometries (described by Z or H/D) and for expected values of η obtained from the geometric non-linear analysis. Normalized hyperbolas for all the open tank models are depicted in Fig. 12(b),

Table 7
Normalized factor for cone roof tank models.

Model	H/D	η	$\overline{\rho}^*$
MC2	0.63	0.606	0.3082
MC4	0.79	0.603	0.3316
MC6	0.95	0.605	0.3205

where each model is characterized by a different curve and a different knock-down factor. However, for all the curves, the normalizing factor is defined by an almost constant value of $\overline{\rho}^*$.

The same normalization was implemented in three models of cone roof tanks. Particularly, for models MC2, MC4 and MC6, Table 7 and Fig. 13(a) summarize the computed values of $\overline{\rho}^*$, which remain almost constant at about 0.32 for all models. Different from the case of the open tanks models, notice that in Table 7, the knock-down factor η is practically the same. Additionally, the normalized hyperbolas shown in Fig. 13(b) are almost coincident. The cause may be that the models considered have similar deflected patterns in the buckled zone, which in turn have the same thickness configuration and lead to almost identical classical eigenvalues. Also, the non-linear behavior is similar for the three models as illustrated previously in Fig. 5.

From this proposed normalization in the range ψ^C–ρ^C, it is possible to see that the change from the classical eigenmode to the reduced eigenmode (obtained in this case from a geometrically non-linear analysis) follows a uniform pattern described

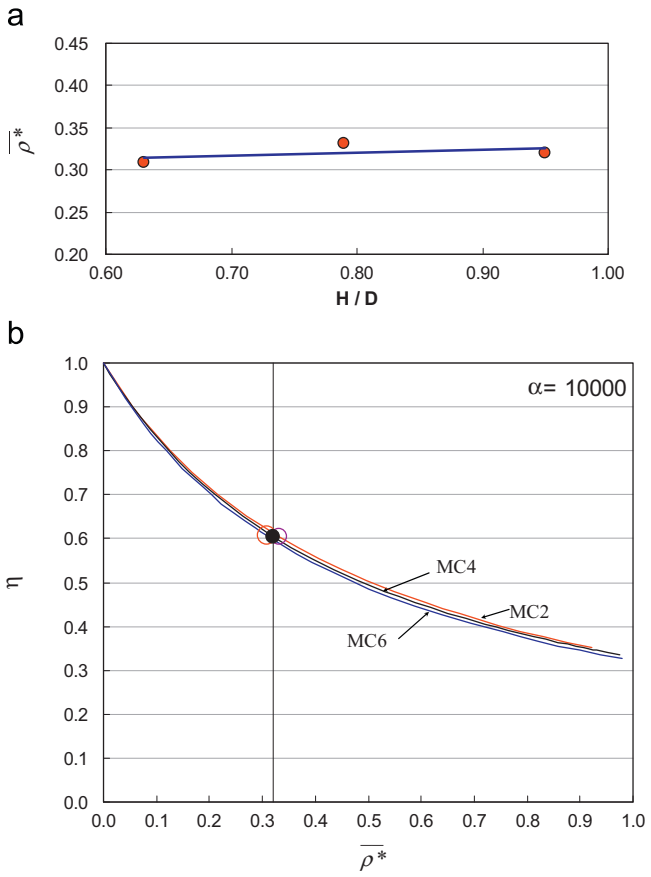

Fig. 13. (a) Variation of $\overline{\rho}*$ as a function of H/D. (b) Variation of η as a function of $\overline{\rho}*$, for selected cone roof tank models.

by the uniformity in the values of $\overline{\rho}^*$. These values indicate the fraction necessary to add to the classical ρ^C to obtain the true ρ^* and consequently the right knock-down factor η for each model.

Clearly, in this alternative procedure to improve the results obtained previously for wind pressures, it is necessary to compute a non-linear path for a high amplitude imperfection (typically $\xi/t=1$ or 2) in order to determine the mode and the maximum load reached for that level of imperfection. Furthermore, the procedure requires computing the energy for the reduced membrane stiffness in addition to computing energies using the classical eigenmode. All these operations were done here to understand the reason for the differences in the results on models under wind loads, but they cannot be implemented as a standard simple procedure to find the knock-down factor for the classical buckling load. This is a limitation of the method described in [15] and it restricts its applicability to those cases in which the classical eigenmode is quite similar to the reduced energy mode.

5. Conclusions

From the results obtained in the previous sections using a general purpose finite element code and a lower bound buckling formulation, it is possible to obtain a preliminary general conclusion. The proposed reduced energy method is not able to estimate the lower bound for wind pressures. For cone roof tanks, the non-linear imperfection-sensitivity analysis shows results that are similar for all models, but with a tendency to estimate a lower critical load than that predicted by the reduced energy method. Although the differences in the knock-down factors are not significant (about 10%), the lower bound predicted by the reduced energy method is unsafe for design.

The differences in the results for open top models are more important. Significant discrepancies were found in comparison with a non-linear analysis. The main source of the discrepancies seems to be the shape of the mode used in the computations of the energy. This feature was verified from the geometrically non-linear analysis, and it is seen that the modal shape changes from the full membrane stiffness configuration to the reduced membrane configuration. This change in the modal shapes seems to invalidate one of the main assumptions made in the formulation of the reduced energy method, namely that the buckling mode in the lower bound is the same as in the unreduced membrane stiffness state. Considering those observations, an attempt to apply an alternative way to improve the method using a code like Abaqus requires at least one additional condition to find the correct knock-down factor. However such a condition is not available from the proposed formulation or requires additional computations that are useful to understand the differences in the results but are beyond the purpose of implementing the reduced energy method for wind loads in a simple way.

Acknowledgements

The second author thanks Prof. James G. A. Croll, who introduced him to the Reduced Stiffness approach and to Dr. Rossana Jaca for many fruitful discussions on the implementation of the method. Support from the National University of Cordoba and CONICETis gratefully acknowledged.

References

[1] Godoy LA. Performance of storage tanks in oil facilities following Hurricanes Katrina and Rita. ASCE Journal Performance of Constructed Facilities 2007;21(6):441–9.
[2] Jaca R, Godoy LA. Wind buckling of metal tanks during their construction. Thin Walled Structures 2010;48:453–9.
[3] Koiter WT, On the stability of elastic equilibrium. PhD thesis. Delft (in Dutch with English summary), H.J. Paris, Amsterdam, 1945.
[4] Greiner R, Derler P. Effect of imperfections on wind loaded cylindrical shells. Thin-Walled Structures 1995;23(1–4):271–81.
[5] Greiner R. Cylindrical shells: wind loading. London: EFN Spon; 1998. [Chapter 17 in Silos].
[6] Jerath S, Sadid H. Buckling of orthotropic cylinders due to wind load. Journal of Engineering Mechanics, ASCE 1985;111(5):610–22.
[7] Godoy LA, Flores FG. Imperfection sensitivity to elastic buckling of wind loaded open cylindrical tanks. Structural Engineering and Mechanics 2002;13(5):533–42.
[8] Flores FG, Godoy LA. Buckling of short tanks due to hurricanes. Engineering and Structures 1998;20(8):752–60.
[9] Portela G, Godoy LA. Wind pressures and buckling of cylindrical steel tanks with conical roof. Journal of Construction Steel Research 2005;61(6):786–807.
[10] Croll JGA. Towards a rationally based elastic–plastic shell buckling design methodology. Thin-Walled Structures 1995;23(1):67–84.
[11] Croll JGA, Batista R. Explicit lower bounds for buckling of axially loaded cylinders. International Journal of Mechanical Science 1981;23(1):333–43.
[12] Croll JGA, Ellinas CP. Reduced stiffness axial buckling of cylinders. International Journal of Solid Structures 1983;19(5):461–77.
[13] Yamada S, Croll JGA, Croll JGA. Buckling and post-buckling characteristics of pressure-loaded cylinders. Journal of Applied Mechanics, ASME 1993;60(1):290–9.
[14] Yamada S, Croll JGA. Contributions to understanding the behavior of axially compressed cylinders. Journal of Applied Mechanics, ASME 1999;66(1):299–309.
[15] Sosa EM, Godoy LA, Croll JGA. Computation of lower bound buckling loads using general-purpose finite element codes. Computers and Structures 2006;84:1934–45.
[16] Jaca RC, Godoy LA, Flores FG, Croll JGA. A reduced stiffness approach for the buckling of open cylindrical tanks under wind pressure. Thin-Walled Structures 2007;45(9):727–36.
[17] API Standard 650. Welded steel tanks for oil storage. Washington, D.C: American Petroleum Institute; 1988.

[18] MacDonald PA, Kwok KCS, Holmes JD. Wind loads on circular storage bins and tanks: I. point pressure measurements on isolated structures. Journal of Wind Engineering and Industrial Aerodynamics 1988;31(1):165–88.
[19] Abaqus. User's Manuals, Version 6.3. Rhode Island: Hibbitt, Karlsson and Sorensen, Inc.; 2002.
[20] Batoz JL, Bathe KJ, Ho LW. A study of three-node triangular plate bending elements. International Journal for Numerical Methods in Engineering 1980;15(1):1771–821.
[21] ASCE-7-02. Minimum design loads for buildings and other structures. Reston, VA: ASCE; 2002.